15

Synthesis, Characterization, Toxicity of Nanomaterials for Biomedical Applications

A. K. Pradhan, K. Zhang, M. Bahoura, J. Pradhan,
P. Ravichandran, R. Gopikrishnan and G. T. Ramesh
Norfolk State University,
United State of America

1. Introduction

Nanomaterials are widely used for biomedical applications as their sizes are comparable with most of the biological entities. Many diagnostic and therapeutic techniques based on nanoscience and nanotechnologies are already in the clinical trial stages, and encouraging results have been reported. The progress in nanoscience and nanotechnology has led to the formation and development of a new field, nanomedicine, which is generally defined as the biomedical applications of nanoscience and nanotechnology. Nanomedicine stands at the boundaries between physical, chemical, biological and medical sciences, and the advances in nanomedicine have made it possible to analyze and treat biological systems at the cell and sub-cell levels, providing revolutionary approaches for the diagnosis, prevention and treatment of some fatal diseases, such as cancer. Nanomagnetism is at the forefront of nanoscience and nanotechnology, and in the field of nanomedicine, magnetic nanomaterials are among the most promising for clinical diagnostic and therapeutic applications. Similarly, luminescent materials are equally important for tagging and imaging applications.

The nanomaterials used for biomedical purposes generally include zero-dimensional nanoparticles, one-dimensional nanowires and nanotubes, and two-dimensional thin films. For example, magnetic nanoparticles and nanotubes are widely used for labeling and manipulating biomolecules, targeting drugs and genes, magnetic resonance imaging (MRI), as well as hyperthermia treatment. Magnetic thin films are often used in the development of nanosensors and nanosystems for analyzing biomolecules and diagnosing diseases. As the synthesis and characterization of these nanostructures are completely interdisciplinary, there is a need of coordinated efforts for the successful implementation of these nanomaterials. The synthesis of nanoparticles with required shape, size, and core-shell configuration (surface coating) along with proper characterization are still in the early stage of research. On the other hand, due to the similar size to biological systems, nanoparticles pose potential threats to health and they could consequently have a large impact on industry and society. Hence, apart from successful synthesis and characterization of various nanomaterials, an effort to understand the toxicological impacts of nanomaterials much research has to be done to establish standards and protocols for the safe use of nanomaterials in industry as well as in the public arena, including academia and research laboratories.

Nanoparticles have sparked intense interest in anticipation that this unexplored range of material dimensions will yield size-dependent properties. The physical and chemical

properties vary drastically with size and use of ultra fine particles clearly represents a fertile field for materials research. The modern biology and biomedical science have stepped into the molecular level. Effectively probing biological entities and monitoring their biological processes are still a challenge for both basic science investigation and practical diagnostic/therapeutic purposes. Since nanomaterials possessing analogous dimensions to those of functional aggregates organized from biomolecules they are believed to be a promising candidate interface owing to their enhanced interaction with biological entities at the nano scale (Whitesides, 2003). For this reason, nanocrystals with advanced magnetic or optical properties have been actively pursued for potential biomedical applications, including integrated imaging, diagnosis, drug delivery and therapy (Lewin et al., 2000; Hirsch et. al., 2003; Alivisatos, 2004; Kim et. al., 2004; Liao and Hafner, 2005). The development of novel biomedical technologies involving *in vivo* use of nanoparticles present multidisciplinary attempts to overcome the major chemotherapeutic drawback related to its spatial nonspecificity. For example, in most biomedical and magnetofluidic applications, magnetic nanoparticles of fairly uniform size and Curie temperature above room temperature are required. On the other hand, as the major advantage of nanotubes, the inner surface and outer surface of nanotubes can be modified differently due to their multi-functionalization. While the inner surface was tailored for better encapsulation of proper drugs, the outer surface can be adjusted for targeted accessing. On the other hand, the strong magnetic behavior made maghemite nanotubes easier controlled by a magnetic field, especially compared with hematite nanotubes. Mainly due to their tubular structure and magnetism, magnetic nanotubes are among the most promising candidates of multifunctional nanomaterials for clinical diagnostic and therapeutic applications. The tubular structure of magnetic nanotubes provides an obvious advantage as their distinctive inner and outer surfaces can be differently functionalized, and the magnetic properties of magnetic nanotubes can be used to facilitate and enhance the bio-interactions between the magnetic nanotubes and their biological targets (Son et. al., 2009; Liu et. al., 2009). One application paradigm of magnetic nanotubes is drug and gene delivery (Plank et. al., 2003). One of the major applications of magnetic nanomaterials is targeted drug delivery. In chemotherapies, to improve the treatment efficiency and decrease or eliminate the adverse effects on the healthy tissues in the vicinity of a tumor, it is practically desirable to reduce or eliminate undesirable drug release before reaching the target site, and it is really critical that the drugs are released truly after reaching the target site, in a controllable manner via external stimuli (Satarkar & Hilt, 2008; Chertok et. al., 2008; Hu et. al., 2008; Liu et. al., 2009). This remains one of the important fields of research for the development of smart drug carriers, whose drug release profiles can be controlled by external magnetic fields, for example the drug to be released is enclosed in a magnetic-sensitive composite shell.

With rapid development of nanotechnology and handling of nanoparticles in various industrial and research and medical laboratories, it is expected that the number of people handling nanoparticles could double in few years from now putting more urge towards its safe use (Tsuji et. al. 2005). However, knowing the potential use and burden of exposure, there is little evidence to suggest that the exposure of workers from the production of nanoparticles has been adequately assessed (Shvedova et. al., 2003; Tsuji et. al. 2005). Despite these impressive, futuristic, possibilities, one must be attentive to unanticipated environmental and health hazards. In view of the above, the exposure to nanoparticles and nanotubes could trigger serious effects including death, if proper safety measures are not taken. Few findings from published articles certainly justify a moratorium on research

involving nanoparticles, if not all nanoparticles, until proper safeguards can be put in place, moreover safety tests need to be carried out keeping in view the type of nanomaterials present. Currently, the literature surveys on suggested nanotoxicity are few to draw any conclusion on the exposure dose of nanoparticles required for toxicity.

2. Eu^{3+} doped Gd_2O_3 luminescent nanostructures

The nanoscale structures, which include nanoparticles, nanorods, nanowires, nanotubes and nanobelts (He et. al., 2003; Chang et. al., 2005; Li et. al., 2007; Mao, et. al., 2008; Zhang et al., 2009), have been considerably investigated due to their unique optical, electronic properties and prospective application in diverse fields, such as high quality luminescent devices, catalysts, sensors, biological labeling and other new functional optoelectronic devices. The precise architectural manipulation of nanomaterials with well-defined morphologies and accurately tunable sizes remains a research focus and a challenging issue due to the fact that the properties of the materials closely interrelate with geometrical factors such as shape, dimensionality, and size. The properties and performances of nanostructures strongly depend on their dimensions, size, and morphologies (Liu et. al., 2007). Therefore, synthesis, growth, and control of morphology in the crystallization process of nanostructures are of critical importance for the development of novel technologies.

Rare earth doped oxides are promising new class of luminescent material due to their electronic and optical properties that arises from their 4f electrons. Therefore, much attention has been paid to their luminescent characteristics such as their large stokes shift, sharp emission visible spectra, long fluorescence lifetime (1-2 ms), and lack of photo-bleaching compared with dyes (Wang et. al., 2005; Nichkova et. al., 2006). These materials, especially in the nanostructure, have been widely used in the lighting industry and biotechnology, including plasma display panel, magnetic resonance imaging enhancement, and microarray immunoassays for fluorescence labels (Seo et. al., 2002; Nichkova et. al., 2005; Bridot et. al., 2007; Petoral et. al., 2009). Since the morphology and dimensionality of nanostructures are of vital factors, which particularly have an effect on the physical, chemical, optical, and electronic properties of materials, it is expected that rare earth doped oxides synthesized in the form of nanoscale may take on novel spectroscopic properties of both dimension controlled and modified ion-phonon confinement effect compared to their bulk counterparts. Gd_2O_3, as a rare earth oxide, is a useful paramagnetic material and good luminescent rare earth doped host. Eu^{3+} ions can be doped into Gd_2O_3 easily since they are all trivalent ions and have the same crystal structure. Furthermore, $^5D_0$ -$^7F_2$ of Eu^{3+} transitions exhibit red characteristic luminescence at a wavelength of 611 nm. Therefore, lanthanide oxide doped nanostructures can be used as electrical, magnetic or optical multifunction materials.

Recently, considerable efforts have been made to synthesize low dimensional nanostructures (Chang et. al., 2005; Li et. al., 2007; Liu et. al., 2008). However, these processes have to be involved in hydrothermal routine, template, and catalysts. The nanostructure formed depends somehow on the pressure, template, and catalysts. This results in experimental complexity, impurities, defects and high cost. In addition, these methods especially could not meet large scale produce in industry. Therefore, it is necessary to find new methods to synthesize shape, size, and dimensionality controlled lanthanide doped oxides. On the other hand, because of the distinct low effective density, high specific

surface area, and encapsulation ability in hollow nanotubes these nanostructures are exceptionally promising in various fields such as confined catalysis, biotechnology, photonic devices, and electrochemical cells (Xu & Asher, 2004; Lou et. al., 2006; Wei et. al., 2008). Although lanthanide oxides are excellent host lattices for the luminescence of various optically active lanthanide ions (Mao et. al., 2009), Gd_2O_3 is a promising host matrix for down- and up conversion luminescence because of its good chemical durability, thermal stability, and low phonon energy (Yang et. al., 2007; Jia et. al., 2009).

3. Synthesis of Gd_2O_3: Eu^{+3} nanostructures

Gd_2O_3 doped with Eu^{3+} nanostructures were synthesized by either sol-gel or co-precipitation wet chemical solution methods. Nanoparticles were synthesized by a sol-gel method from their acetate hydrate precursors, which were dissolved in water. This solution was mixed with citric acid solution in 1:1 volume ratio ultrasonically for about 30 min. The mixture was heated in a water bath at 80 °C until all water is evaporated, yielding a yellowish transparent gel. The gel was further heated in an oven at 100 °C which formed a foamy precursor. This precursor decomposed to give brown-colored flakes of extremely fine particle size on further heating at 400 °C for 4 h. The flakes were ground and sintered at 800 °C for duration of 2 h. Further heating in O_2 ambient removed the carbon content.

The nanoparticles of Eu:Gd_2O_3 were coated by adopting a base-catalyzed sol-gel process. 100 mg of Eu:Gd_2O_3 were dispersed in 20 ml of 2-propanol solution and sonicated for 30 min. 75 µl of tetraethoxysilane (TEOS) and 25 µL of 25% NH_3H_2O solution were injected into the above mixture and sonicated for 30 min at 60 ^oC. By means of centrifugation the suspended silica capsulated Eu:Gd_2O_3 were obtained. The coated particles were washed several times by using acetone and methanol in order to remove any excess unreacted chemicals. The purified powder was naturally dried. This procedure produces a very uniform SiO_2 coating, as determined using a transmission electron microscope (TEM). By changing the formulation of the coating solution, we can control the coating thickness.

In the co-precipitation method, 0.5 M aqueous solution was prepared by dissolving $Gd(NO_3)_3$ and $Eu(NO_3)_3$ in deionized H_2O. The nitrate solutions with cationic molar ratio of Gd to Eu is 0.95: 0.05 were mixed together and stirred for 30 minutes. The aqueous solution of 0.2 M NH_4HCO_3 was prepared and mixed with the nitrate solution drop wise while stirring to form the precipitate. It is noted that in this experiment extra 10 mol% NH_4HCO_3 was added in order to ensure all the rare earth ions reacted completely to obtain rare earth carbonates. The white precipitate slurry obtained was aged for 24 hours at room temperature with continuous stirring. Then the precipitates were centrifugated and washed with deionized water for 5 times in order to completely remove NO^{3-}, NH^{4+} and HCO^{3-} followed by drying at about 75 ^oC in the stove. After drying, the white precursor was ground several times. It is noted that the dried precursor powders were very loosely agglomerated and can be pulverized very easily. To get Gd_2O_3 doped with Eu^{3+} nanostructures, the as-synthesized samples were further calcined at 600, 800, and 1000 ^oC in air for 2 hours in the furnace, respectively.

Eu^{3+} doped Gd_2O_3 nanotubes were synthesized according to a modified wet chemical method (He et. al., 2003). A mixture of 30 ml of 0.08 M $Gd(NO_3)_3$ and $Eu(NO_3)_3$ with a nominal molar ratio of Eu/Gd 5 atom %, in a form of clear solution, were added into flasks through ultrasound for 10 min. 30 ml of 25 wt % of ammonia solution was added quickly

into the solution under vigorous stirring for 20 min. Meanwhile, the pH value of the mixture was measured which came to a value of about 10. The mixture was heated under vigorous stirring in a 70 ^{o}C silicon oil bath for 16 hours. After this procedure, a white precipitate precursor was obtained. The final as-prepared precipitates were separated by centrifugation, washed with deionized water and ethanol for 4 times, respectively, and dried for 12 hours at 65 ^{o}C in air to get as-grown sample. To get Gd_2O_3 product, the as-synthesized samples were further annealed in air for 2 hours at 600 ^{o}C in the furnace.

Figure 1 (a-c) shows the representative TEM morphologies of Eu:Gd_2O_3 nanoparticles. The size distribution is rather narrow, and the nanocrytallite size is in the range of 20-30 nm for as-prepared nanoparticles by citric-gel technique. However, the nanoparticles are slightly agglomerated. The particle sizes increase to 30-40 nm if the nanoparticles are calcined up to 800 ^{o}C. Figure 1 (c) represents the TEM image of Eu:Gd_2O_3 nanoparticle coated by SiO_2 indicating distinctly well dispersed nanoparticles. It is noted that the size of the SiO_2 shell can be controlled by controlling TEOS and NH_3H_2O solution.

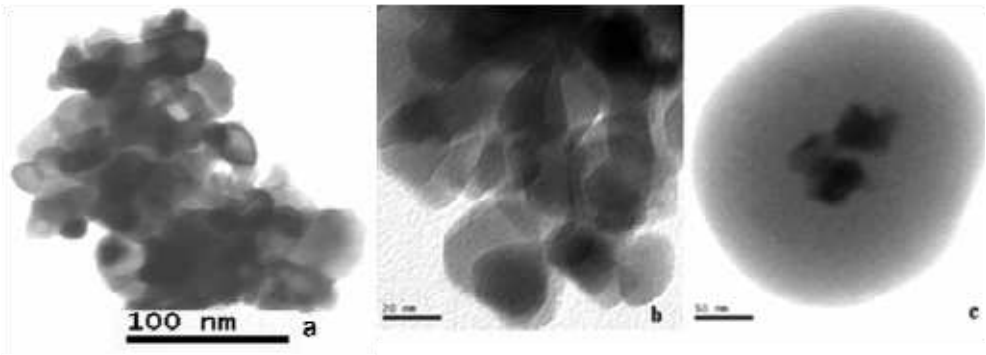

Fig. 1. Transmission electron microscopy (TEM) image of Eu:Gd2O3 nanopowders of (a) as prepared, (b) calcined at 800 ^{o}C and (c) SiO2 coated.

Figure 2 shows the emission spectra of citric-gel technique synthesized Eu doped Gd_2O_3 nanoparticles. The photoluminescence spectrum illustrates the Eu^{3+} ions are in cubic symmetry and indicate the characteristics of red luminescent Eu:Gd_2O_3, in which the $^5D_0 \rightarrow {}^7F_2$ transition at about 611 nm is prominent, and the relatively weak emissions at the shorter wavelengths are due to the $^5D_0 \rightarrow {}^7F_1$ transitions. The cubic structure provides two sites, C_2 and S_6, from two different crystalline sites, in which the $^5D_0 \rightarrow {}^7F_2$ transition originates from the C_2 site of the electric dipole moment of Eu^{3+} ions that scarcely arises for the S_6 site because of the strict inversion symmetry. This suggests that the emission emerges mainly from the C_2 site in the cubic structure. The emission spectra show similar characteristics after SiO_2 coating on the surface of Eu:Gd_2O_3 nanoparticles. This clearly suggests that the emission properties of Eu ions remain intact even after SiO_2 coating, and can be utilized for biomedical tagging.

Figure 3 shows the magnetic moment of Eu:Gd_2O_3 and SiO_2 coated Eu:Gd_2O_3 nanoparticles at 300 K. Both nanoparticles demonstrate paramagnetic behavior at room temperature. On the other hand, the coated nanoparticles showed reduced magnetization compared to Eu:Gd_2O_3 due to reduction in the volume fraction caused by SiO_2 coating.

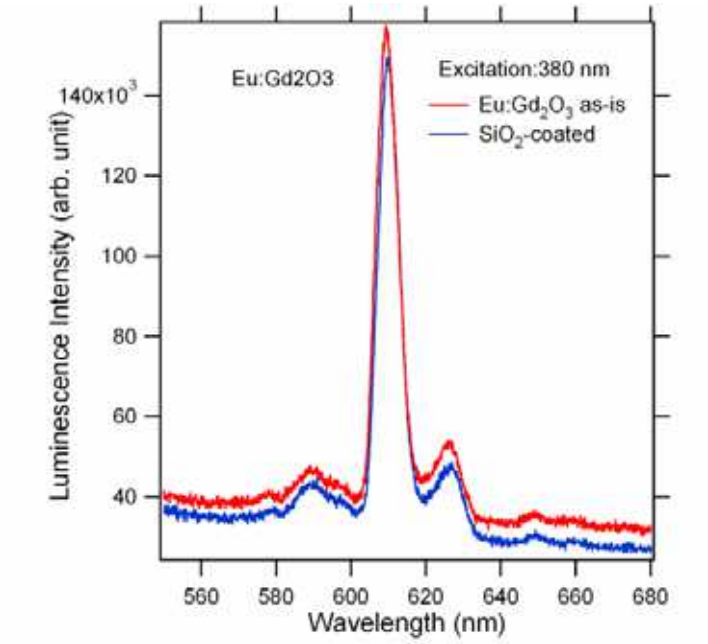

Fig. 2. Photoluminescence of $Eu:Gd_2O_3$ nanoparticles calcined at 800 ^{0}C.

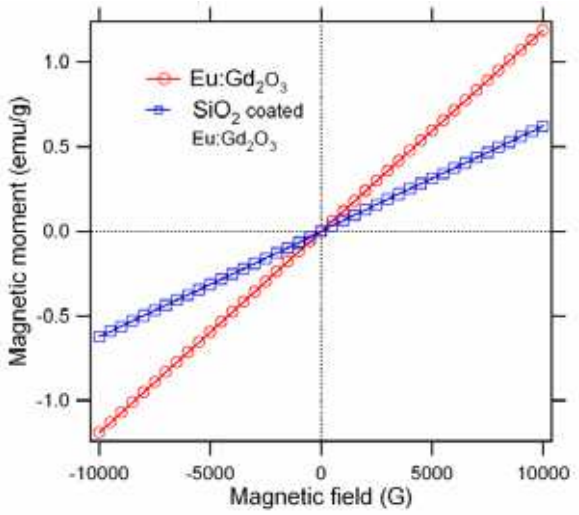

Fig. 3. Magnetic moment of $Eu:Gd_2O_3$ and SiO_2 coated $Eu:Gd_2O_3$ nanoparticles.

The morphology of Eu^{3+} doped Gd_2O_3 nanorods obtained after calcination at 600 ^{o}C for 2 hours strongly depends on the heat treatment temperature. The formation of nanorods with low aspect ratio is preferred at 600 ^{o}C. It can be seen from the micrograph that all the nanorods display uniform morphology having size of 10 nm in diameter and more than 300

nm in length (Figure 4(a)). In contrast, the nanorods grow bigger in diameter (about 25 nm) and shorter in length (about 100 nm) after the heat treatment at 800 °C as shown in Figure 4(c). However, it is evident that Eu^{3+} doped Gd_2O_3 nanorods maintain the anisotropic shape during heat treatment from 600 °C to 800 °C. It can also be observed that the formation of nanorods is related to the fact that the growth direction are preferred along the [211] crystallographic orientation. This is because the spacing between fringes along nanorod axes is about 0.40 nm which is close to the interplanar distance of the cubic (211) plane as shown in Figure 4 (b) and (d). Figure 4(e) presents the TEM images of Eu^{3+} doped Gd_2O_3 nanoparticles with size of 60 nm in diameter obtained by heat treatment at 1000 °C. The morphology of Eu^{3+} doped Gd_2O_3 nanostructure dependent on the heat treatment temperature is possibly attributed to meta-stable states which are able to recrystallize at 1000 °C. A favorable growth pattern parallel to the (222) plain corresponding to interplanar spacing of 0.3 nm dominates the recrystallization of nanorods and transFigures to form nanoparticles as shown in Figure 4(f).

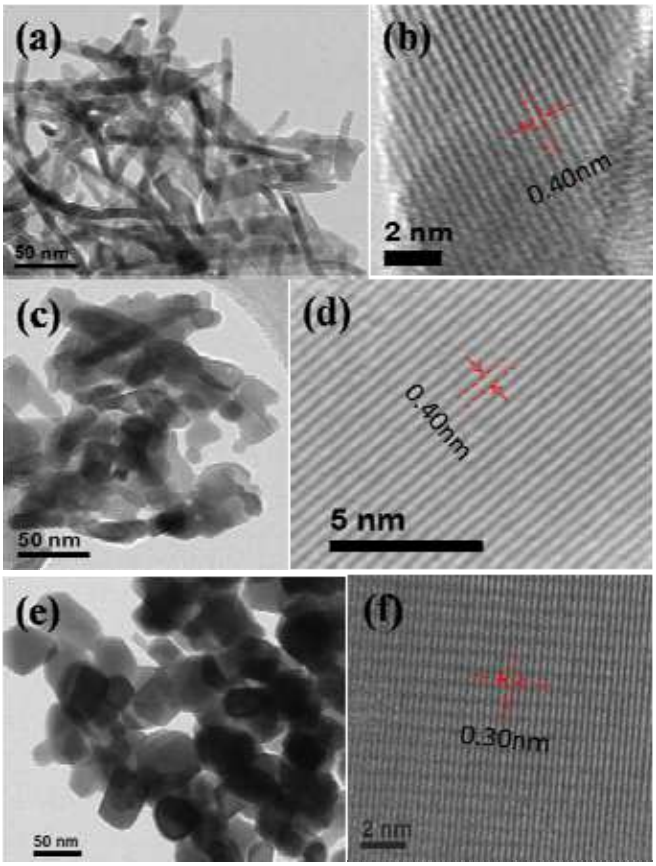

Fig. 4. Eu^{3+} doped Gd_2O_3 nanostructures TEM photographs of low and high magnification after annealing at (a) and (b) 600 °C, (c) and (d) 800 °C, and (e) and (f) 1000 °C, respectively.(b), (d) and (f) represent the HR-TEM images of respective nanostructures.

The optical properties and characteristics of nanostructures used in the photonic application are typically determined by their dimensions, size, and morphologies. The intensity of photoluminescence of Eu^{3+} doped Gd_2O_3 nanorods strongly depends on the annealing temperature at which the morphology of nanostructures gets modified. Figure 5 shows the emission spectra of Eu^{3+} doped Gd_2O_3 nanorods excited by 263 nm ultraviolet light.

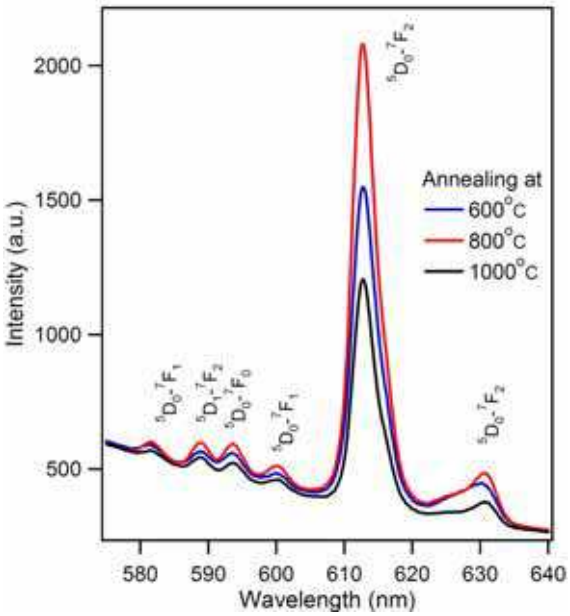

Fig. 5. Photoluminescence spectra of Eu^{3+} doped Gd_2O_3 nanostructures annealing at 600 °C, 800 °C, and 1000 °C, respectively.

The emission spectra exhibit a strong red emission characteristic of the $^5D_0$-$^7F_2$ (around 613 nm) transition which is an electric-dipole-allowed transition. The weaker band around 581 nm, 589 nm, 593 nm, 600 nm and 630 nm are ascribed to $^5D_0$-$^7F_1$, $^5D_1$-$^7F_2$, $^5D_0$-$^7F_0$, $^5D_0$-$^7F_1$, and $^5D_0$-$^7F_2$, respectively (Liu et. al., 2008). The emission spectra indicates that the Eu^{3+} doped Gd_2O_3 nanostructures represent strong, narrow, and sharp emission peaks. As shown in Figure 5, the intensity of emission at 613 nm of nanorods increases when the annealing temperature increases from 600 °C to 800 °C modifying the morphology of the nanorods as described earlier. However, when the annealing temperature reaches 1000 °C, the emission intensity is reduced significantly, even less than the one annealed at 600 °C. The performance change of photoluminescence in these nanostructures can be attributed to the morphological transformation of the nanostructures as described below. At low annealing temperature, the Eu^{3+} doped Gd_2O_3 exhibits nanorod morphology with more surface area containing a larger number of luminescent centers. However, when the temperature was increased to 1000 °C, the nanorods transformed to nanoparticles which have more surface area altogether. This increase in surface area resulted in more defects, especially surface defects and strains, located on the surface of the nanoparticles. Although high annealing temperature can increase crystal perfection, the defects on the surface of these nanoparticles can overwhelm, causing reduced photoluminescence.

In order to systematically investigate the correlation of morphology and optical characteristics of Eu^{3+} doped Gd_2O_3 samples, the 5 at.% Eu^{3+} doped Gd_2O_3 nanorods fabricated at 600 ^oC were used. Representative TEM and SEM images of Eu^{3+} doped Gd_2O_3 nanotubes are shown in Figure 6. It can be observed these nanostructures demonstrate tubular shape with a length in the range about 0.7-1 μm and the wall thickness of 20 nm. It also reveals that these one dimension nanostructures have open ends, smooth surface and straight morphology as shown in Figure 6 (a) and (b). Figure 6(c) demonstrates the Field Emission-Scanning Microscope (FE-SEM) image large number of uniform nanotubes. The open end and the associated fine feature, such as uniform size and shape, of these nanotubes are shown in the inset of Figure 6.

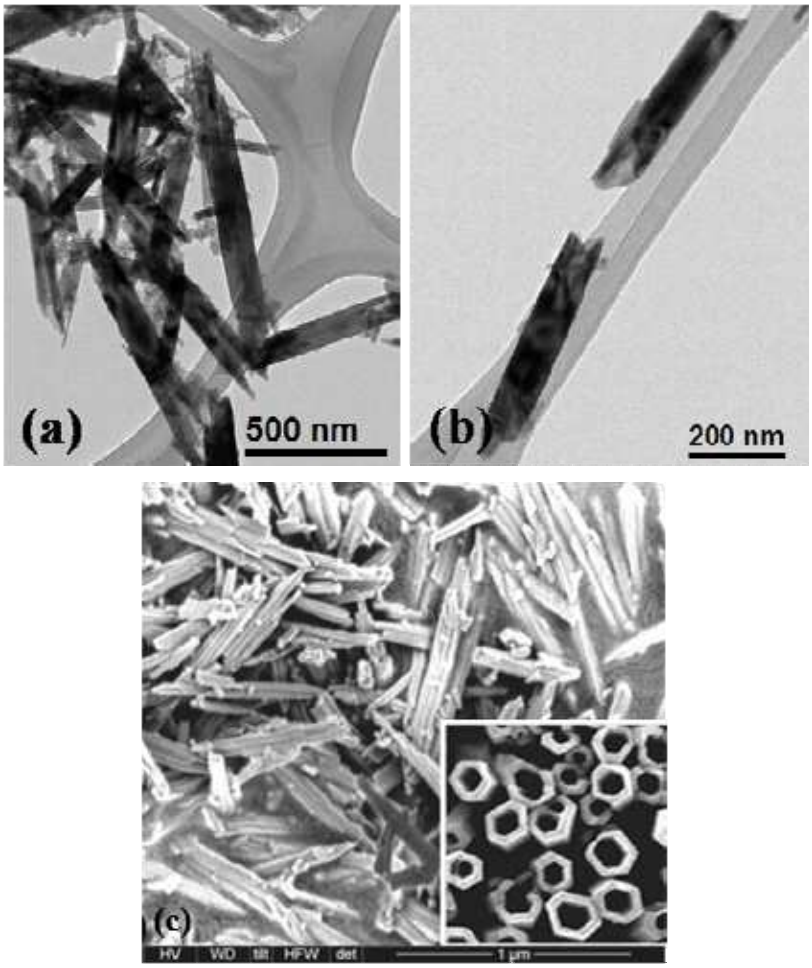

Fig. 6. (a) and (b) Low magnification TEM photographs and (c) FE-SEM images of Eu^{3+} doped Gd_2O_3 nanotubes after annealing at 600 ^oC. The inset in (c) demonstrates the nanotube feature of Eu^{3+} doped Gd_2O_3.

It is obviously revealed that the emission intensity of nanotubes is larger than the nanorods of Eu^{3+} doped Gd_2O_3 samples as shown in Figure 7. Nanotubes have more surface area than the nanorods. It is worth mentioning that the emission measurements were performed with a very similar conditions and volume fractions of nanomaterials used in this study. Although, the number of defects increases with the increase of area in nanotubes, the layer surface area overwhelms the luminescent intensity.

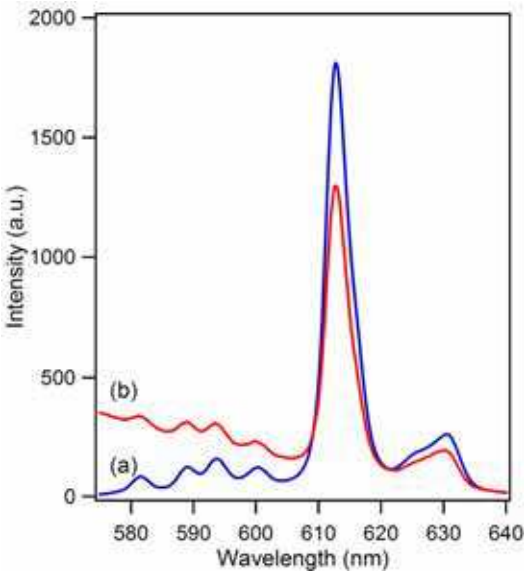

Fig. 7. Photoluminescence spectra comparison of Eu^{3+} doped Gd_2O_3 nanotubes (a) and nanorods (b) annealed at 600 ^oC, respectively.

4. ZnO nanostructures

Zinc oxide (ZnO) is a semiconductor material with various configurations, much richer than of any other known nanomaterial (Pradhan et. al., 2006; Ma et. al., 2007). At nanoscale, it posses unique electronic and optoelectronic properties and finds application as biosensors, sunscreens, as well as in medical applications like dental filling materials and wound healing (Ghoshal et. al., 2006). Because of the indiscriminate use of ZnO nanoparticles, it is important to look at their biocompatibility with biological system. A recent study on ZnO reports that it induces much greater cytotoxicity than non-metal nanoparticles on primary mouse embryo fibroblast cells (Yang et. al., 2009), and induces apoptosis in neural stem cell (Deng et. al., 2009). Published reports have shown that ZnO inhibits the seed germination and root growth (Lin & Xing, 2007); exhibit antibacterial properties towards *Bacillus subtilis* and to a lesser extent to *Escherichia coli* (Adams et. al., 2006). Inhalation of ZnO compromises pulmonary function in pigs and causes pulmonary impairment and metal fume fever in humans (Fine et. al., 1997; Beckett et. al., 2005). Literature evidences showed that ZnO nanoparticles are the most toxic nanoparticle with the lowest LD50 value among the engineered metal oxide nanoparticles (Hu et. al., 2009). On the other hand, it was also reported that zinc oxide was not found to be cytotoxic to cultured human dermal fibroblasts

(Zaveri et. al., 2009). In recent years, there has been an escalation in the development of techniques for synthesis of nanorods and subsequent surface functionalization. ZnO nanorods exhibit characteristic electronic, optical, and catalytic properties significantly different from other nano metals. Keeping in view of the unique properties and the extensive use of ZnO in many fields and also contradictory results on ZnO toxicity from both in-vitro and in-vivo studies, we report here to synthesize and characterize the ZnO nanorods on hela cells for its biocompatibility/toxicity.

5. Synthesis: ZnO nanotubes

The typical method employed is as follows. Equal volume of 0.1 M aqueous Zinc acetate anhydrous and Hexamethylenetetramine were mixed in a beaker using ultrasonication for 30 min. After the mixture was mixed well, it was heated at 80 °C in water bath for 75 min, during which white precipitates were deposited at the bottom. Then it was incubated for 30 min in ice cold water to terminate the reaction. The product was washed several times (till the pH of solution becomes neutral) using the centrifuge with deionized water and alcohol, alternatively to remove any by-product and excess of hexamethyleneteteamine. After washing, the solution was centrifuged at 10,000 rpm (12,000×*g*) for 20 min and the settled ZnO was dried at 80 ◦C for 2 h.

Fig. 8 (a, b) shows the SEM micrograph collected on synthesized ZnO nanorods surface morphology. The nanorod was grown perpendicular to the long-axis of the matrix rod and grew along the [001] direction, which is the nature of ZnO growth. The morphology of ZnO nanorod was further confirmed by the TEM image as shown in Fig. 8 (c, d). Though the rod cores were monodisperse, the length of the nanorod was estimated to be around 21 nm in diameter and the length around 50 nm.

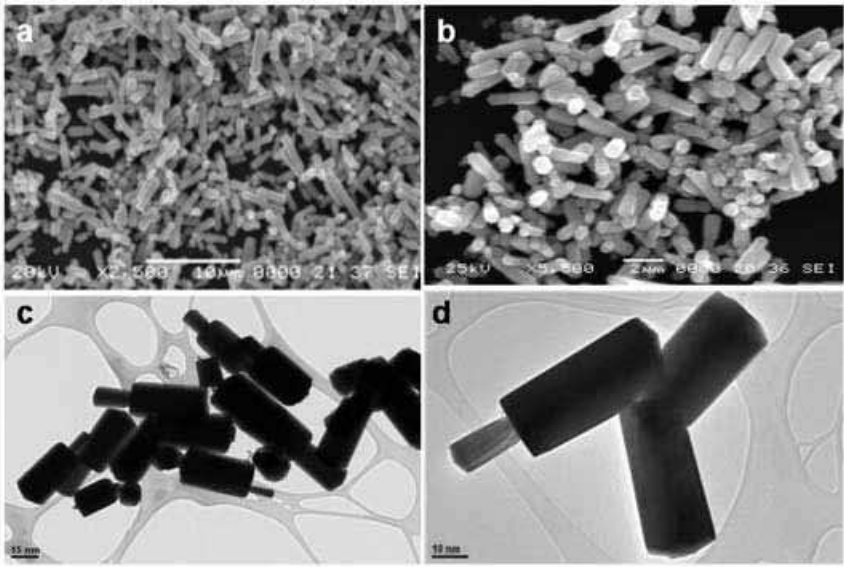

Fig. 8. (a and b) Scanning electron micrograph of ZnO nanorods. (c and d) Transmission electron micrograph of ZnO nanorods.

6. Toxicity studies: Eu:Gd_2O_3 nanoparticles

For cell culture and treatments, rat lung epithelial cell line (LE, RL 65, ATCC; CRL- 10354) from ATTC was grown at 37 °C in an atmosphere of 5% CO_2 and in complete growth medium supplemented with 1% penicillin/streptomycin and 10% fetal bovine serum (FBS). Eu:Gd_2O_3 were suspended in Dimethyl formamide (DMF) and sonicated for 5 minutes and henceforth in all control experiments the cells were treated with equivalent volume of DMF. The cells were incubated with or without nanoparticles in 96 well plates for time intervals as indicated in the respective Figure legends.

The measurements of intracellular reactive oxygen species (ROS) were performed in the following way. Oxygen radicals collectively called as reactive oxygen species play a key role in cytotoxicity. Increased ROS levels in cells by chemical compounds reflect toxicity and cell death. To study the induction of oxidative stress in LE cells, $1x10^4$ cells/well were seeded in 96 well plate and grown overnight under standard culture conditions. The cells were then treated with 10 μM of dichlorofluorescein [5-(and-6)-carboxy-2,7`-dichloro-dihydroxyfluorescein diacetate, H_2DCFDA, (C-400, Molecular Probes, Eugene, OR) for 3 h in Hank's balanced salt solution (HBSS) in incubator. Following 3 h of incubation, cells were washed with phosphate buffered saline (PBS) and treated with different concentrations of Eu:Gd_2O_3 nanoparticles. Following incubation the intensity of fluorescence is measured at different time intervals at excitation and emission of wavelength at 485/527 nm, respectively and expressed as fluorescence units.

LE cells were seeded at $5x10^3$ cells/well in a 96 well plate and allowed to grow overnight. After 18 h in serum-free medium, cells were treated with different concentrations of nanoparticles and grown for 72 h. At the end of the incubation, cells were additionally treated with 3-[4, 5-dimethylthiazol- 2-yl]-2,5-diphenyltetrazolium bromide] MTT for 3 h. The cells were then washed with chilled PBS and formazon formed was solubilized in 100 μL of acidic propanol and the absorbance was read at 570 nm.

The results of the toxicity test are presented in Fig. 9. The cytotoxicity assay was essentially performed as described elsewhere (Zveri et. al., 2009). Figure 9 indicates the effect of coated and uncoated Eu:Gd_2O_3 on rat LE cells suggesting that they induce ROS in a dose dependent manner. Uncoated Eu:Gd_2O_3 increased ROS by 0.5 folds as compared to control at a concentration as low as 2.5 μg were as coated Eu:Gd_2O_3 showed 1 fold increase in ROS. Coated and uncoated Eu:Gd_2O_3 induces very less ROS. To study the extent of damage caused by coated and uncoated Eu:Gd_2O_3 on cell viability, MTT assay was carried in LE cells treated with various concentrations and the results suggest that the cell viability decreases with increase in concentration of nanoparticles by 72 hrs compared to control. It was found that 60% of cells found to be viable at 2.5μg/ml of uncoated Eu:Gd_2O_3 where as 50% found to be viable with cells treated with coated Eu:Gd_2O_3. In all, measurement of intracellular reactive oxygen species and MTT assay results show that Eu:Gd_2O_3 nanoparticles are relatively nontoxic and the toxicity is further decreased on SiO_2 coating (Zhang et. al., 2009).

7. Toxicity studies of ZnO nanorods

Hela cells, which are immortalized cervical cancer cells, are used for the testing of ZnO nanorods. Hela cells were treated with different concentration (0.5, 1.0, 2.0, 2.5, 5.0,10

µg/ml) of ZnO nanorods for 3 h. They showed no significant induction of ROS (Fig. 10 a**).** Earlier studies on different nanoparticles such as single and multi walled carbon nanotubes showed significantly increased levels of ROS at 5-10µg/ml (Manna et. al., 2005; Sarkar et. al., 2007; Ravichandran et. al., 2009), whereas no increase in ROS level even in 20µg/ml was detected in ZnO nanorods. The time kinetics was also performed to check the formation of ROS (Fig. 10 b). It is seen that there is no significant ROS level formed as early as 30 min with 10µg/ml of ZnO nanorods and remained same till 150 min is passed. However, at later time intervals the increase in ROS was observed in 10µg/ml but very less as compared to the control. This may be due to osmotic pressure created by excess of nanorods. Next, the level of lipid peroxidation in ZnO nanorods exposed hela cells was investigated. This is another possible player for oxidative stress induction. It was observed that very minimal (as low as 0.1 fold) increase in lipid peroxidation level with 10µg/ml of ZnO nanorods as compared to the control.

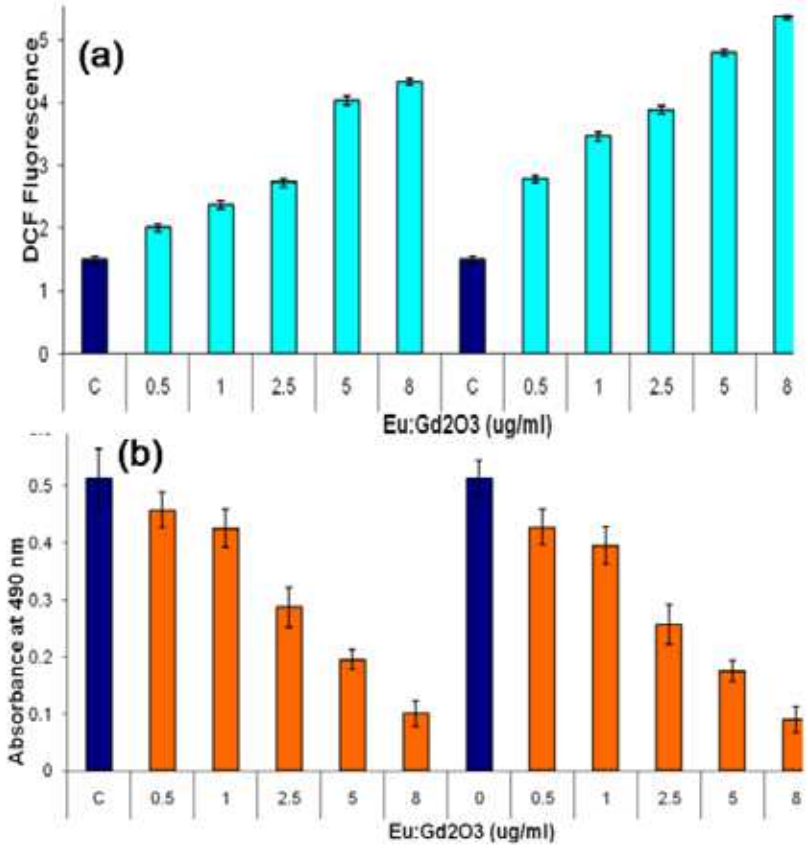

Fig. 9. (a) Uncoated (left) and coated (right) Eu:Gd_2O_3 induces ROS in rat LE cells, and (b) MTT assay effect of uncoated (left) and coated (right) Eu:Gd_2O_3 on cell viability.

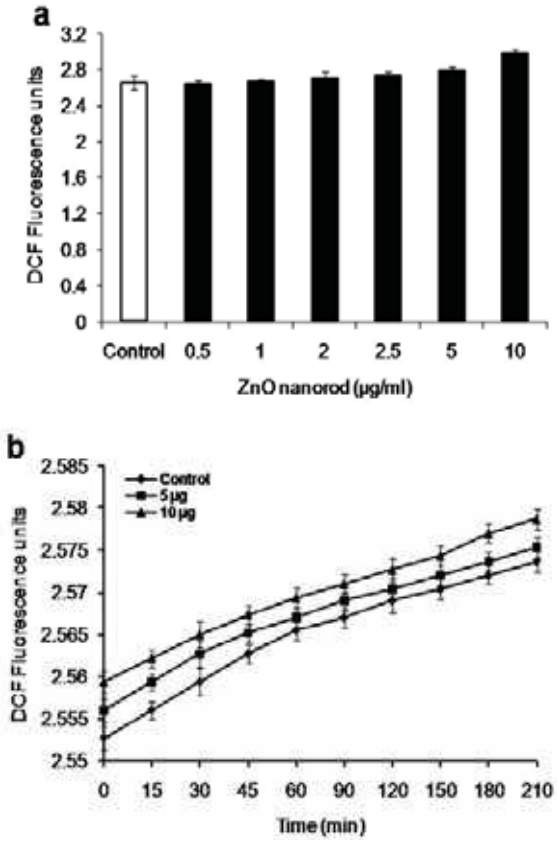

Fig. 10. Effect of ZnO nanorods on oxidative stress. Equal numbers of 1×105 hela cells/well were grown for 18 h. (a) The grown cells were incubated with 10 µM of DCF for 3 h, treated with different concentration of ZnO nanorods. Fluorescence was measured at excitation and emission wavelengths of 485 and 527 nm, respectively, at the end of 3 h. (b) Time kinetics of ROS formation by ZnO nanorods. Overnight grown hela cells were treated with 1, 5, and 10 µg/ml of ZnO nanorods. Fluorescence was measured at excitation and emission wavelengths of 485 and 527 nm, respectively, at different time points. The values are expressed as DCF fluorescence units, mean ± SD of eight wells and the Figure is a representative of three experiments performed independently

In order to check whether ZnO nanorod has any role on toxicity without altering oxidative stress, analysis of cell damage using MTT assay after exposing to various concentration of ZnO nanorods (0.5, 1.0, 2, 2.5, 5.0, 10 µg/ml) (Fig. 11a) was performed. The MTT assay showed no significant decrease in cell viability suggesting that ZnO nanorods did not have any effect on cell toxicity. More than 98% of cells were viable at concentration of 10 µg/ml ZnO nanorods which is also confirmed by live dead cell assay (Fig. 11b). 50% of cell death was observed in mouse neuroblastoma cells using 100 µg/ml of ZnO (Prasad et. al., 2006), whereas other reports have also shown 100% cytotoxicity at 15 µg/ml of ZnO on mesothelioma MSTO-211H or rodent 3T3 fibroblast cells (Brunner et. al., 2006), and 90% cell

death with 20mgL−1 of ZnO nanoparticles on HELF cells (Yuan et. al., 2010). Also, 5 mM of ZnO nanoparticle are shown to be less toxic to human T cells (Reddy et. al., 2007). Previous studies from our laboratory on hela cells and other cells such as lung epithelial, H1299, A549 and HaCaT cells showed the decrease in cell viability at 5 µg/ml when they were exposed to SWCNT and MWCNT (Manna et. al., 2005; Sarkar et. al., 2007; Ravichandran et. al., 2009). Toxicological studies on hela cells and conclude that ZnO nanorods could be the safe nanomaterials (Gopikrishnan el. al., 2010) for biological applications.

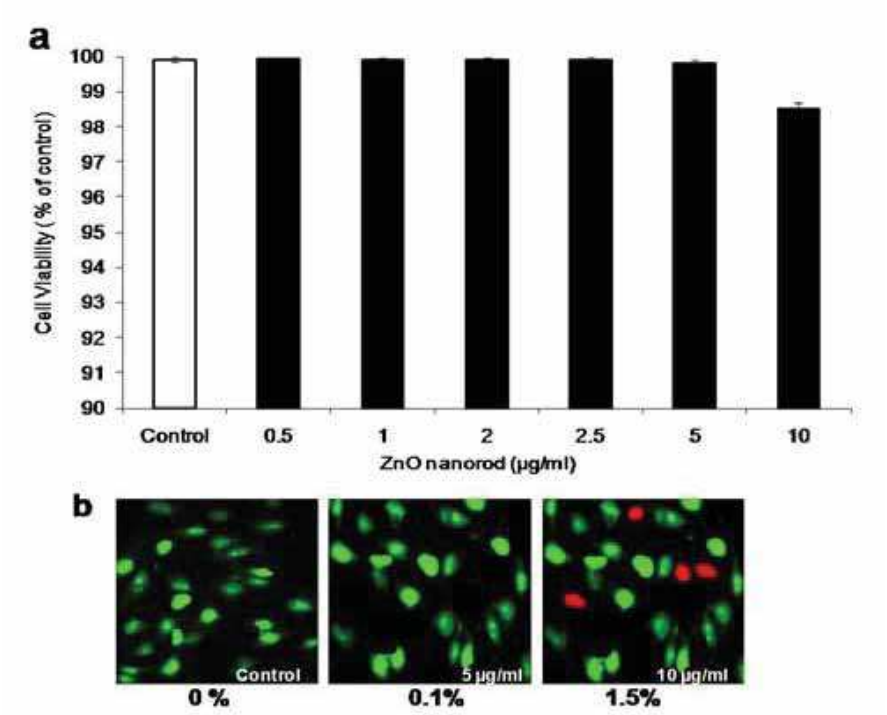

Fig. 11. Effect of ZnO nanorods on cell viability. HeLa cells (2000/well in a 96-well plate) were incubated for 12 h and treated with different concentration of ZnO nanorods for 72h. (a) Cell viability was assayed by MTT dye uptake. The mean absorbance at 570 nm is represented as cell viability percentage of the control and is mean ± SD of eight wells. (b) HeLa cells were treated with 5 µg/ ml and10 µg/ml of ZnO nanorods for 72 h and the dead cell (red color) numbers were counted. The percentage of dead cells is indicated below each photograph.

8. Magnetic nanoparticles

8.1 Synthesis: LaSrMnO nanoparticles

$La_{0.7}Sr_{0.3}MnO_3$ nanoparticles were synthesized by a sol-gel method from their acetate hydrate precursors, which were dissolved in water (Pradhan el. al., 2008; Zhang el. al., 2010). This solution was mixed with citric acid solution in 1:1 volume ratio ultrasonically for about 30 min. The mixture was heated in a water bath at 80 °C until all water is evaporated,

yielding a yellowish transparent gel. The gel was further heated in an oven at 100 °C which formed a foamy precursor. This precursor was decomposed to give black-colored flakes of extremely fine particle size on further heating at 400 °C for 4 h. The flakes were ground and sintered at 800 °C for duration of 2 h. Further heating in O_2 ambient removed the carbon content. The ball milling was used with methanol to reduce the size of nanoparticles of LSMO (Fig. 12). The solution containing suspended LSMO nanoparticles was separated using ultra-high centrifuge using methanol for several times.

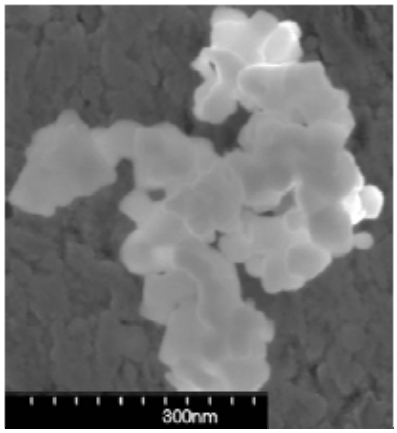

Fig. 12. FE-EM image of LSMO nanoparticles annealed at 800 ^{o}C, showing the individual nanoparticles.

The nanoparticles of ball milled LSMO were coated by adopting a base-catalyzed sol-gel process. 100 mg of LSMO were dispersed in 20 ml of 2-propanol solution and sonicated for 30 min and the nanoparticles were shown in Fig. 13 (a). 75 µl of TEOS and 25 µL of 25% NH_3H_2O solution were injected into the above mixture and sonicated for 30 min at 60 ^{o}C. The suspended silica capsulated LSMO nanoparticles were obtained by means of centrifugation. The coated nanoparticles were washed several times by using acetone and methanol in order to remove any excess unreacted chemicals. The purified powder was naturally dried. This procedure produces a very uniform SiO_2 coating, as determined using a transmission electron microscope. By changing the formulation of the coating solution, the coating thickness can be controlled.

8.2 FeCo nanoparticles

FeCo nanoparticles were synthesized by a coprecipitation method under Ar atmosphere from their chloride hydrate precursors. The FeCo nanopowders were dried in Ar gas, and were dispersed in 2- propanol solvent with 10^{-2} M and sonicated for 1 hour followed by addition of TEOS and 25% ammonia solution of volume ration 3:1. The mixture was sonicated for 1 h to coat the SiO_2 onto the surface of FeCo nanoparticles. The solution containing suspended FeCo-SiO_2 nanoparticles was decanted and purified using methanol several times in order to remove unreacted Fe and organic materials from the surface. The coated nanopowders were naturally dried in air. Figure 14 (a) shows XRD pattern of the as-synthesized samples, indicating typical amorphous phase. The amorphous phase in FeCo nanoparticles is generated because the coprecipitation reaction takes place below the glass

transition temperature and boron atoms are presented in the nanoparticles. The solution containing suspended FeCo-SiO_2 nanoparticles was decanted and purified using methanol several times in order to remove unreacted Fe and organic materials from the surface. The coated nanopowders were naturally dried in air.

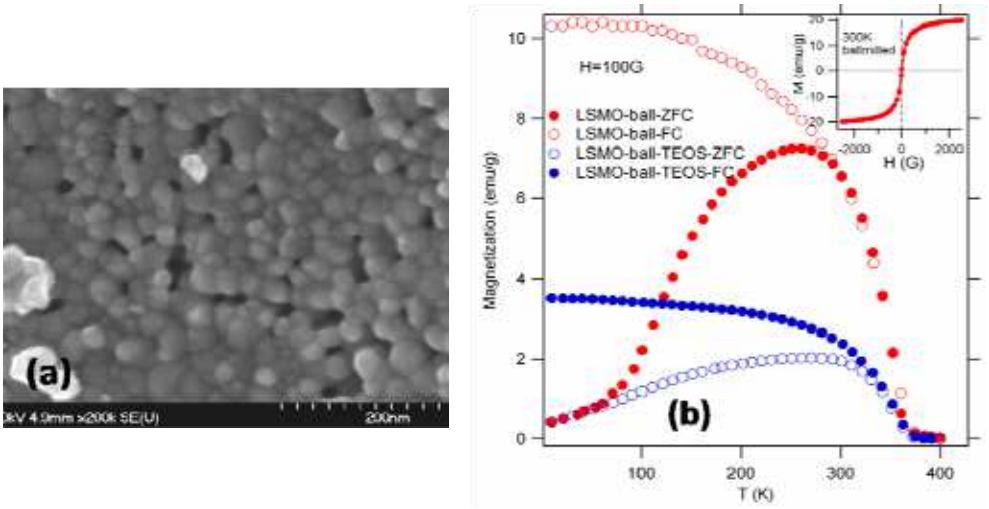

Fig. 13. (a) FE-SEM image of ball-milled LSMO nanopowder. (b) Temperature dependence of FC and ZFC magnetization of ballmilled and TEOS-coated nanoparticles. The inset shows the MH curve for ball-milled sample at 300 K.

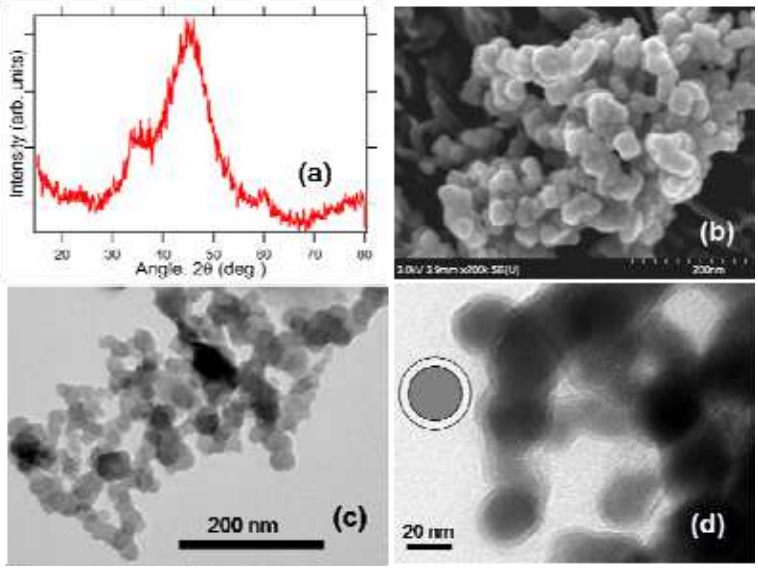

Fig. 14. (a) XRD patterns of FeCo nanoparticles prepared for 4 h, (b) FE-SEM and (c) TEM images of as synthesized FeCo nanoparticles, and (d) FeCo nanoparticles coated with silica.

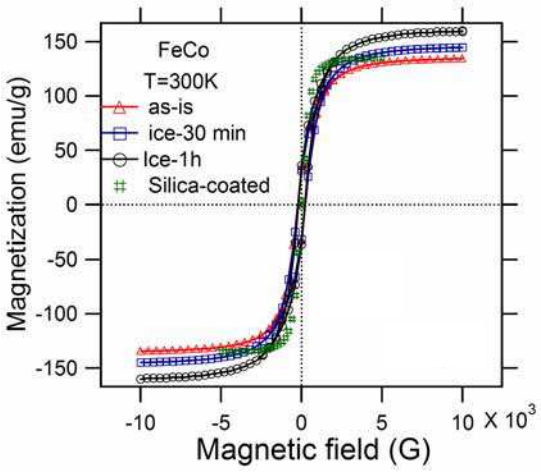

Fig. 15. Magnetization hysteresis loops of FeCo nanoparticles synthesized at various conditions and FeCo nanoparticles coated with silica.

Figure 14 (b) and (c) show the FE-SEM and TEM image of the uncoated FeCo nanoparticles, respectively. The FeCo nanoparticles are spherical in shape with about 20 nm in size and well-dispersed. The size distribution is very uniform, indicating the high-quality of the nanoparticles. Figure 14 (d) shows the TEM image of the silica coated FeCo nanoparticles, exhibiting well-formed FeCo cores with SiO_2 shell of couple of nm. It was realized that the shell diameter can be increased with increasing coating time, concentration and temperature. Figure 15 shows the magnetic hysteresis of FeCo nanoparticles. It is noted that the magnetization saturation moment increases when FeCo nanoparticles are synthesized at lower temperature (such as at ice temperature) due to controlled nucleation compared to as-grown nanoparticles. The magnetization of silica coated FeCo decreases, mainly due to the reduction in the demagnetization factor among nanoparticles through coupling, which is generally induced through direct exchange coupling and dipolar interaction. The magnetization reduction in coated FeCo is not significant, illustrating a strong dipolar exchange coupling.

9. Toxicity of magnetic nanoparticles

9.1 LSMO nanoparticles

The effect of LSMO and silica-coated LSMO NPs on reactive oxygen species were measured by a real time assay. To study the induction of oxidative stress in lung epithelial (LE) cells, $1x10^4$ cells/well were seeded in 96 well plate and grown overnight under standard culture conditions. The cells were then treated with 10 μM of dichlorofluorescein [5-(and-6)-carboxy-2, 7-dichloro-dihydroxyXuorescein diacetate, H_2DCFDA, (C-400, Molecular Probes, Eugene, OR)] for 3 h in Hank's balanced salt solution (HBSS) in incubator. Following 3 h of incubation, cells were washed with phosphate buffered saline (PBS) and 5 μg, 10 μg and 60 μg of LSMO and Si coated-LSMO NPs was added respectively and incubated at 37 °C. Cells were incubated in an incubator for 3 h as detailed in the Figure caption of Fig. 16, and fluorescence was measured at excitation wavelength of 485 nm and emission was recorded at 527 nm (Thermo Lab Systems, Franklin, MA). It is very clear from Fig. 16 that silica-coated LSMO NPs generate less oxidative stress in LE cells compared to uncoated NPs.

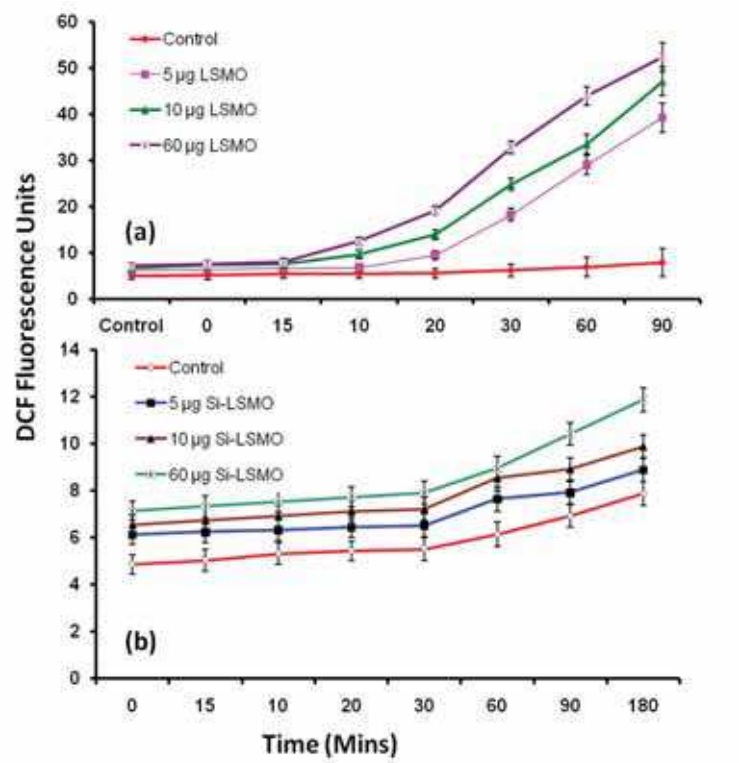

Fig. 16. Effects of magnetic nanoparticles on time kinetics of ROS in LE cells. (a) LSMO generates oxidative stress in LE cells. 1x10^5 cells/well were seeded in a 96 well plate and grown at standard conditions for 24 h. Following overnight incubation, cells were starved in serum free medium for 24 h. Then cells were washed with phosphate buffered saline and incubated with 10 µM DCF for 3 h in HBSS. The cells were then treated with 5, 10 and 60 µg of LSMO. The change in DCF fluorescence was measured at 485 and 527 nm respectively after each time interval as shown. Values are mean ± SD of eight wells and are a representative from three experiments performed independently. (b) Silicon coated LSMO generates less oxidative stress in LE cells using the experiment described in (a).

The cytotoxicity assay was essentially performed as described earlier. The LE cells were seeded at 5x10^3 cells/well in a 96 well plate and grown overnight. After 18 h in serum-free medium, cells were treated with different concentrations of LSMO and Si coated-LSMO and grown for 72 h. At the end of the incubation, cells were additionally treated with 3-[4, 5-dimethylthiazol- 2-yl]-2,5-diphenyltetrazolium bromide] MTT for 3 h. The cells were then washed with chilled PBS and formazon formed was extracted in 150 µL of acidic methanol and the absorbance was read at 570 nM. Fig. 17 demonstrates that the silica-coated LSMO NPs have better cell viability compared to uncoated NPs.

The above cytotoxicity tests (ROS and cell viability) demonstrate that LSMO nanoparticles can be potential candidate for various biomedical applications. Further perfection can be made achieved by coating the nanoparticles with silica in a controlled way. Apart from *in*

vivo biomedical applications, LSMO nanoparticles can also be utilized in protein purification due to their size-dependent magnetic properties, where large size (> 50 nm) NPs show strong ferromagnetic properties at room temperature. The LSMO nanoparticles may be complementary to paramagnetic nanoparticles composed of Ni and NiO (Rodríguez-Llamazares et. al, 2008; Wong et. al., 2008). The *in situ* modification of the surface during the precipitation (Wong et. al., 2008) used for LSMO nanoparticles becomes very effective in reducing the cytotoxicity.

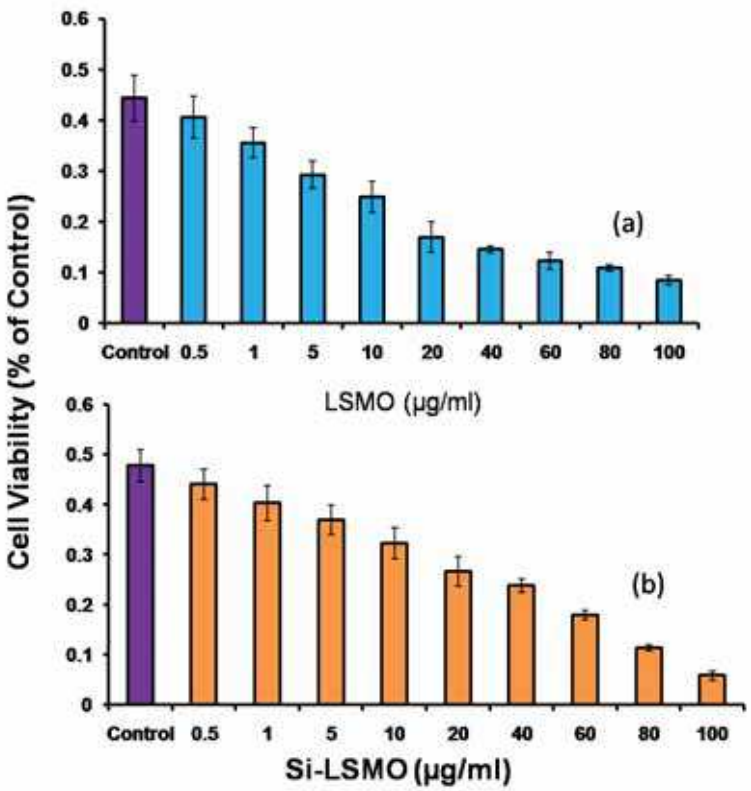

Fig. 17. Effect of magnetic nanoparticles on cell viability. (a) LSMO decreases cell viability in LE cells. 2000 cells/well were seeded in a 96 well and grown under standard condition for 24 h. Following overnight incubation, cells were starved in serum free medium for 24 h. Cells were then treated with 0.5, 1, 5, 10, 20, 40, 60, 80 and 100 µg of LSMO and allowed to grow for 72 h. The MTT assay was then performed. The mean absorbance at 570 nm is represented as percent of control and is mean ± SD of eight wells. The values are a representative from three experiments performed independently. (b) Effect of silica-coated LSMO cell viability using the procedure described in (a).

9.2 FeCo nanoparticles

The result of the toxicity test is presented in Fig. 18. The effect of FeCo and silica-coated FeCo nanoparticles on rat LE cells suggests that they induce ROS in a dose dependent

manner. Uncoated FeCo nanoparticles increased ROS by 3.2 folds as compared to control at a concentration as low as 2.5 µg. The coated FeCo nanoparticles showed 3.6 fold increase in ROS (Fig. 18 (b)). To study the extent of damage caused by coated and uncoated FeCo on cell viability, MTT assay was carried in LE cells treated with various concentrations and the results suggest that the cell viability decrease with increase in concentration of FeCo nanoparticles by 72 hrs compared to control. Only 40% of cells found to be viable at 2.5 µg/ml of uncoated FeCo, where as 35% found to be silica-coated FeCo nanoparticles. This suggests that the silica shell thickness should be increased in order to reduce the toxicity of FeCo nanoparticles for any biomedical applications.

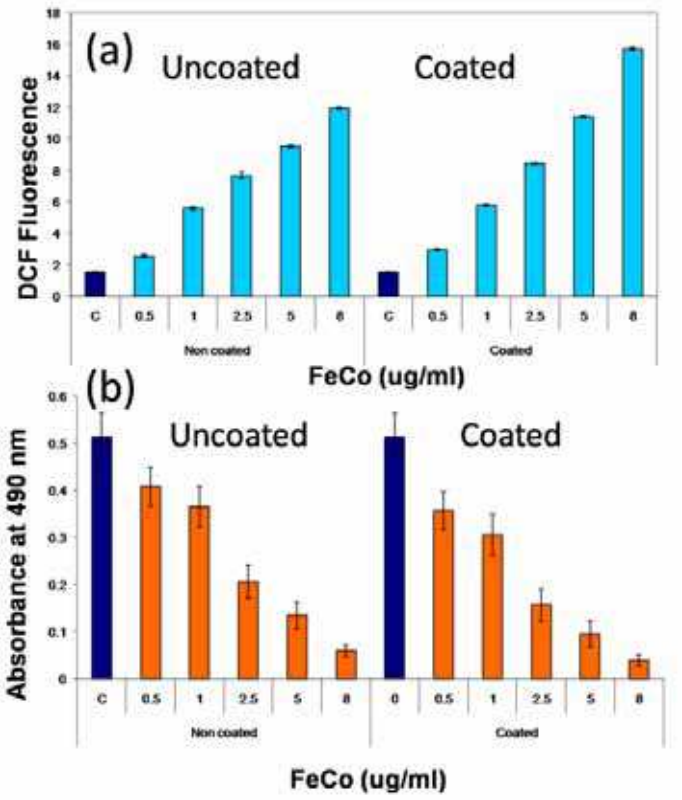

Fig. 18. MTT assay effect of (a) uncoated and (b) coated FeCo nanoparticles on cell viability.

10. Conclusion

Nanomaterials are widely used for biomedical applications because their sizes are comparable with most of the biological entities. The development of novel biomedical technologies involving *in vivo* use of nanoparticles presents multidisciplinary attempts to overcome the major chemotherapeutic drawbacks. Nanomaterials stand at the boundaries between physical, chemical, biological and medical sciences, and the advances in this field impact analyzing and treating biological systems at the cell and sub-cell levels, providing

revolutionary approaches for the diagnosis, prevention and treatment of some fatal diseases, such as cancer. However, the synthesis, characterization and use of these nanomaterials need thorough studies. The synthesis and characterization of several kinds of nanomaterials, such as luminescent, semiconducting and magnetic, are discussed. The toxicity associated with these nanomaterials is also discussed.

Luminescent nanostructures. Eu^{3+} doped Gd_2O_3 nanomaterials are very promising luminescent as well as magnetic material. Some typical growth process for varieties of nanostructures, such as nanoparticles, nanorods, nanotubes and encapsulated nanoparticles, are described with some insight into their microstructures and their optical and magnetic properties. The toxicity studies of some of these nanostructures demonstrate that $Eu:Gd_2O_3$ nanoparticles are relatively nontoxic and the toxicity is further decreased on silica coating.

Semiconductor nanostructures. A typical chemical route was explored to synthesize large scale ZnO nanorods with about 21 nm in diameter and 50 nm in length. Toxicological studies on hela cells show that ZnO nanorods could be the safe nanomaterials for biological applications.

Magnetic nanostructures. Manganites and FeCo nanoparticles were synthesized by the chemical technique and the nanostructures were coated with TEOS and other macromolecules. The manganites display essential magnetic properties applicable for hyperthermia applications. On the other hand, FeCo nanoparticles display strong magnetism appropriate for protein purification.

The cytotoxicity tests (ROS and cell viability) demonstrate that both manganites and FeCo nanoparticles can be potential candidate for various biomedical applications. Further perfection can be made achieved by coating the nanoparticles with silica in a controlled way. The silica shell thickness should be increased in order to reduce the toxicity of FeCo nanoparticles for any biomedical applications.

11. Acknowledgments

This work is supported by the NSF for Research Infrastructure in Science and Education (RISE) grant No. HRD-0734846 and RISE-HRD-0931373. The authors are thankful to T. Holloway for experimental help.

12. References

Adams, L. K.; Lyon, D. Y. & Alvarez, P. J. (2006). Comparative eco-toxicity of nanoscale TiO_2, SiO_2, and ZnO water suspensions**.** *Water Research*, 40, 19, pp. 3527-3532 (November 2006), ISSN 0043-1354

Alivisatos, P. (2004). The use of nanocrystals in biological detection. *Nature Biotechnology*, 22,1, (January 2004) pp. 47–52, ISSN 1087-0156

Beckett, W. S.; Chalupa, D. F.; Pauly-Brown, A.; Speers, D. M.; Stewart, D. J.; Frampton, M. W.; Utell, D. J.; Huang, L. S.; Cox, C.; Zareba, W. & Oberdorster, G. (2005). Comparing Inhaled Ultrafine vs Fine Zinc Oxide Particles in Healthy Adults:A Human Inhalation Study. *American Journal of Respiratory and Critical Care Medicine*, 171, 10, (May 2005) pp. 1129-1135, ISSN 1073-449X

Bridot, J.-L.; Faure, A.-C.; Laurent, S.; Rivière, C.; Billotey, C.; Hiba, B.; Janier, M.; Josserand, V.; Coll, J.-L.; Vander Elst, L.; Muller, R.; Roux, S.; Perriat, P. & Tillement, O. (2007). Hybrid gadolinium oxide nanoparticles: multimodal contrast agent for in vivo

imaging. *Journal of the American Chemical Society*, 129, 16, (March 2007) pp. 5076-5084, ISSN 0002-7863

Brunner, T. J.; Wick, P.; Manser, P.; Spohn, P.; Grass, P. N.; Limbach, L.; Bruinink, A. & Stark, W. J. (2006). In Vitro Cytotoxicity of Oxide Nanoparticles: Comparison to Asbestos, Silica, and the Effect of Particle Solubility. *Environmental Science & Technology*, 40, 14, (March 2006) pp. 4374-4381, ISSN 0013-936X

Chang, C.; Kimura, F.; Kimura, T. & Wada, H. (2005). Preparation and characterization of rod-like Eu:Gd_2O_3 phosphor through a hydrothermal routine. *Materials Letters*, 59, 8-9, (April 2005) 1037-1041, ISSN 0167-577X

Chertok, B; Moffat, B. A.; David, A.E.; Yu F. Q.; Bergemann, C.; Ross, B. D. & Yang, V. C. (2008). Iron oxide nanoparticles as a drug delivery vehicle for MRI monitored magnetic targeting of brain tumors. *Biomaterials*, 29, 4, (February 2008) pp. 487-496, ISSN 0142-9612

Deng, X. Y.; Luan, Q. X.; Chen, W. T.; Wang, Y. L.; Wu, M. H.; Zhang, H. J. & Jiao, Z. (2009). Nanosized zinc oxide particles induce neural stem cell apoptosis. *Nanotechnology*, 20, 11, (February 2009) 115101, ISSN 0957-4484

Dosev, D.; Nichkova, M.; Liu, M.; Guo, B.; Liu, G.; Hammock, B. B. & Kennedy, L. M. (2005). Application of luminescent Eu:Gd_2O_3 nanoparticles to the visualization of protein micropatterns. *Journal of Biomedical Optics*, 10,6, (November 2005) 064006, ISSN 1083-3668

Fine, J. M.; Gordon, T.; Chen, L. C.; Kinney, P.; Falcone, G. & Beckett, W. S. (1997). Metal Fume Fever: Characterization of Clinical and Plasma IL-6 Responses in Controlled Human Exposures to Zinc Oxide Fume at and Below the Threshold Limit Value. Journal of Occupational & Environmental Medicine, 39, 8, (August 1997) pp. 722-726, ISSN 1076-2752

Ghoshal, T.; Kar, S. & Chaudhuri, S. (2006). Synthesis and optical properties of nanometer to micrometer wide hexagonal cones and columns of ZnO. *Journal of Crystal Growth*, 293, 2, (August 2006) pp. 438-446, ISSN: 0022-0248

Gopikrishnan, R.; Zhang, K.; Ravichandran, P.; S. Baluchamy, Ramesh, V.; Biradar, S.; Ramesh, P.; Pradhan, J.; Hall, J. C.; Pradhan, A. K. & Ramesh, G. T. (2010). Synthesis, Characterization and Biocompatibility Studies of Zinc oxide (ZnO) Nanorods for Biomedical Application. *Nano-Micro Letters*, 2, 1, (2010) pp. 27-30, ISSN: 2150-5551

He, Y.; Tian, Y. & Zhu, Y. (2003). Large-scale-synthesis of luminescent Y_2O_3: Eu nanobelts. *Chemistry Letters*, 32, 9, (August 2003) pp. 862-863, ISSN 0366-7022

Hirsch, L. R.; Stafford, R. J.; Bankson, J. A.; Sershen, S. R.; Rivera, B.; Price, R. E.; Hazle, J. D.; Halas, N. J. & West, J. L. (2003). Nanoshell-mediated near-infrared thermal therapy of tumors under magnetic resonance guidance. *Proceedings of the National Academy of Sciences of the United States of America*, 100, 23, (November 2003) pp. 13549–13554, ISSN 1091-6490

Hu, S. H.; Chen, S. Y.; Liu, D. M. & Hsiao, C. S. (2008). Core/single-crystal-shell nanospheres for controlled drug release via a magnetically triggered rupturing mechanism. *Advanced Materials*, 20, 14, (July, 2008) pp. 2690-2695, ISSN 1521-4095

Hu, X.; Cook, S.; Wang, P. & Hwang, H. (2009). In vitro evaluation of cytotoxicity of engineered metal oxide nanoparticles. *Science of The Total Environment*, 407, 8, (April 2009) pp. 3070-3072, ISSN 0048-9697

Jia, G.; Liu, K.; Zheng, Y.; Song, Y.; Yang, M. & You, H. P. (2009). Highly uniform $Gd(OH)_3$ and Gd_2O_3:Eu^{3+} nanotubes: facile synthesis and luminescence properties. *Journal of Physical Chemistry C*, 113,15, (March 2009) pp. 6050-6055, ISSN 1932-7447

Kim, S.; Lim, Y. T.; Soltesz, E. G.; De Grand, A. M.; Lee, J.; Nakayama, A.; Parker, J. A.; Mihaljevic, T.; Laurence, R. G.; Dor, D. M.; Cohn, L. H.; Bawendi, M. G.; & Frangioni, J. V. (2003). Near-infrared fluorescent type II quantum dots for sentinel lymph node mapping. Nature Biotechnology, 22, 1, (December 2003) pp. 93–97, ISSN 1087-0156

Lewin, M.; Carlesso, N.; Tung, C.-H.; Tang, X.-W.; Cory, D.; Scadden, D. T.; & Weissleder, R. (2000). Tat peptide-derivatized magnetic nanoparticles allow in vivo tracking and recovery of progenitor cells. *Nature Biotechnology*, 18, 4, (April 2000) pp. 410–414, ISSN 1087-0156

Li, S.; Song, H.; Yu, H.; Lu, S.; Bai, X.; Pan, G.; Lei, Y.; Fan, L. & Wang, T. (2007). Influence of annealing temperature on photoluminescence characteristics of Gd_2O_3:Eu/AAO nanowires. *Journal of Luminescence*, 122-123, 1, (January-April 2007) pp. 876-878, ISSN 0022-2313

Liao, H. W. & Hafner, J. H. (2005). Gold nanorod bioconjugates. *Chemistry of Materials*, 17, 18, (August 2005) pp. 4636–4641, ISSN 0897-4756

Lin, D. H. & Xing, B. S. (2007). Phytotoxicity of nanoparticles: Inhibition of seed germination and root growth. Environmental Pollution, 150, 2, (November 2007) pp. 243-250, ISSN 0269-7491

Liu, G. X.; Hong, G.Y.; Dong, X.T. & Wang, J.X. (2008). Preparation and characterization of Gd_2O_3:Eu^{3+} luminescence nanotubes. *Journal of Alloys and Compounds*, 466, 1-2, (December 2007) pp. 512–516, ISSN 0925-8388

Liu, L.; Ma, E.; Li, R.; Liu, G. & Chen, X. (2007) Effects of phonon confinement on the luminescence dynamics of Eu^{3+} in Gd_2O_3 nanotubes. *Nanotechnology*, 18, 1, (January 2007) pp. 015403-015407, ISSN 0957-4484

Liu, T. Y.; Hu S. H.; Liu, D. M., Chen, S. Y. & Chen, I. W. (2009). Biomedical nanoparticle carriers with combined thermal and magnetic responses. *Nano Today*, 4, 1, (February 2009) pp. 52-65, ISSN 1748-0132

Lou, X. W.; Wang, Y.; Yuan, C.; Lee, J. Y. & Archer, L. A. (2006). Template-free synthesis of SnO_2 hollow nanostructures with high lithium storage capacity. *Advanced Materials*, 18, 17, (September 2006) pp. 2325-2329, ISSN 1521-4095

Ma, T.; Guo, M.; Zhang, M.; Zhang, Y. & Wang, X. (2007). Density-controlled hydrothermal growth of well-aligned ZnO nanorod arrays. *Nanotechnology*, 18, 3, (January 2007) 035605, ISSN 0957-4484

Manna, S. K.; Sarkar, S.; Barr, J.; Wise, K.; Barrera, E. V.; Jejelowo, O.; Rice-Ficht, A. C. & Ramesh, G. T. (2005). Single-Walled Carbon Nanotube Induces Oxidative Stress and Activates Nuclear Transcription Factor-κB in Human Keratinocytes. *Nano Letters*, 5, 9, (August 2005) pp. 1676-1684, ISSN: 1530-6984

Mao, Y. B.; Tran, T.; Guo, X.; Huang, J. Y.; Shih, C. K.; Wang, K. L. & Chang, J. P. (2009). Luminescence of nanocrystalline erbium-doped yttria. *Advanced Functional Materials*, 19, 5, (March 2009) pp. 748-754, ISSN 1616-3028

Mao, Y.; Huang, J. Y.; Ostroumov, R.; Wang, K. L. & Chang, J. P. (2008). Synthesis and luminescence properties of Erbium-doped Y_2O_3 nanotubes. *Journal of Physical Chemistry C*, 112, 7, (January 2008) pp. 2278-2285, ISSN 1932-7455

Nichkova, M.; Dosev, D.; Gee, S. J.; Hammock, B. D. & Kennedy, I. M. (2005). Microarray immunoassay for phenoxybenzoic acid using polymer encapsulated Eu:Gd_2O_3 nanoparticles as fluorescent labels. *Analytical Chemistry*, 77, 21, (September 2005) pp. 6864-6873, ISSN 0003-2700

Nichkova, M.; Dosev, D.; Perron, R.; Gee, S. J.; Hammock, B. D. & Kennedy, I. M. (2006). Eu^{3+}-doped Gd_2O_3 nanoparticles as reporters for optical detection and visualization

of antibodies patterned by microcontact printing. *Analytical and Bioanalytical Chemistry*, 384, 3, (February 2006) pp. 631-637, ISSN 1618-2642

Petoral Jr., R. M.; Söderlind, F.; Klasson, A.; Suska, A.; Fortin, M. A.; Abrikossova, N.; Selegård, L.; Käll, P.; Engström, M. & Uvdal, K. (2009). Synthesis and characterization of Tb^{3+}-doped Gd_2O_3 nanocrystals: a bifunctional material with combined fluorescent labeling and MRI contrast agent properties. *Journal of Physical, Chemistry C*, 113, 17, (April 2009) pp. 6913-6920, ISSN 1932-7447

Plank, C.; Schillinger, U.; Scherer, F.; Bergemann, C.; Rémy, J. S.; Krötz, F.; Anton, M.; Lausier, J. & Rosenecker, J. (2003). The magnetofection method: using magnetic force to enhance gene delivery. Biological Chemistry, 384, 5, (May 2003) pp. 737-747, ISSN 1431-6730

Pradhan, A.K.; Bah, R.; Konda, R. B.; Mundle, R.; Mustafa, H.; Bamiduro, O.; Rakhimov, R. R.; Wei, Xiaohui; & Sellmyer, D. J. (2008). Synthesis and magnetic characterizations of manganite-based composite nanoparticles for biomedical applications. *Journal of Applied Physics*, 103, 7, (2008) 07F704, ISSN 0021-8979

Pradhan, A.K.; Williams, T.M.; Zhang, K.; Hunter, D.; Dadson, J.B.; Lord, K.; Roy, U.N.; Cui, Y. & Burger, A. (2006). Growth of aligned ZnO Nanorods. *Journal of Nanoscience and Nanotechnology*, 6, 7, (July 2006) pp. 1985-1989, ISSN 1550-7033

Prasad, V.; Souza, C. D.; Yadav, D.; Shaikh, A. J.; & Vigneshwaran, N. (2006). Spectroscopic characterization of zinc oxide nanorods synthesized by solid-state reaction. *Spectrochimica Acta Part A*, 65, 1, (September 2006) pp. 173-178, ISSN 1386-1425

Ravichandran, P.; Periyakaruppan, A.; Sadanandan, B.; Ramesh, V.; Hall, J. C.; Jejelowo, O. and Ramesh, G. T. (2009). Induction of apoptosis in rat lung epithelial cells by multiwalled carbon nanotubes. *Journal of Biochemical and Molecular Toxicology*, 23, 5, (October 2009) pp. 333-344, ISSN 1099-0461

Reddy, K. M.; Feris, K.; Bell, J.; Wingett, D. J.; Hanley, C. & Punnoose, A. (2007). Selective toxicity of zinc oxide nanoparticles to prokaryotic and eukaryotic systems. *Applied Physics Letters*, 90, 21, (May 2007) 213902, ISSN 0003-6951

Rodríguez-Llamazares, S.; Merchán, J.; Olmedo, I.; Marambio, H. P.; Muñoz, J. P.; Jara, P.; Sturm, J. C.; Chornik, B.; Peña, O.; Yutronic, N.; & Kogan, M. J. (2008). Ni/Ni Oxides Nanoparticles with Potential Biomedical Applications Obtained by Displacement of a Nickel-Organometallic Complex. *Journal of Nanoscience and Nanotechnology*, 8, 8, (August 2008) pp. 3820-3827, ISSN 1550-7033

Sarkar, S.; Sharma, C.; Yog, R.; Periakaruppan, A.; Jejelowo, O.; Thomas, R.; Barrer, E. V.; Rice-Ficht, A. C.; Wilson, B. L. & Ramesh, G. T. (2007). Analysis of Stress Responsive Genes Induced by Single-Walled Carbon Nanotubes in BJ Foreskin Cells. Journal of Nanoscience and Nanotechnology, 7, 2, (February 2007) pp. 584-592, ISSN 1550-7033

Satarkar, N. S. & Hilt, J. Z. (2008). Magnetic hydrogel nanocomposites for remote controlled pulsatile drug release. *Journal of Controlled Release*, 130, 3, (September 2008) pp. 246-251, ISSN 0168-3659

Seo, S. Y.; Sohn, K. S.; Park, H. D. & Lee, S. (2002). Optimization of Gd_2O_3-based red phosphors using combinatorial chemistry method. *Journal of the Electrochemical Society*, 149, 1, (December 2002) pp. H12-H18, ISSN 0013-4651

Sharma, C. S.; Sarkar, S.; Periyakaruppan, A.; Barr, J.; Wise, K.; Thomas, R.; Wilson, B. L. & Ramesh, G. T. (2007). *Journal of Nanoscience and Nanotechnology*, 7, 7, (July 2007) pp. 2466-2472, ISSN 1550-7033

Shvedova A. A.; Castranova V.; Kisin E. R.; Schwegler-Berry D.; Murray A. R.; Gandelsman V. Z.; Maynard A. & Baron P. (2003). Exposure to carbon nanotube material: assessment

of nanotube cytotoxicity using human keratinocyte cells. Journal of Toxicology and Environmental Health, Part A, 66, 20, (June 2003) pp. 1909-1926, ISSN 1528-7394

Son, S. J.; Reichel, J.; He, B.; Schuchman, M. & Lee, S. B. (2005). Magnetic nanotubes for magnetic-field-assisted bioseparation, biointeraction, and drug delivery. *Journal of the American Chemical Society*, 127, 20, (April 2005) pp. 7316-7317, ISSN 0002-7863

Tsuji, J. S.; Maynard, A. D.; Howard, P. C.; James, J. T.; Lam, C. W.; Warheit, D. B. & Santamaria, A. B. (2005). Research Strategies for Safety Evaluation of Nanomaterials, Part IV: Risk Assessment of Nanoparticles. *Toxicological Sciences*, 89, 1, (September 2005) pp. 42-50, ISSN 1096-0929

Wang, H.; Uehara, M.; Nakamura, H.; Miyazaki, M. & Maeda, H. (2005). Synthesis of well-dispersed Y2O3:Eu nanocrystlas and self-assembled nanodisks using a simple non-hydrolytic route. Advanced Materials, 17, 20, (October 2005) pp. 2506-2509, ISSN 1521-4095

Wei, W.; Ma, G. H.; Hu, G.; Yu, D.; Mcleish, T.; Su, Z. G. & Shen, Z. Y. (2008). Preparation of hierarchical hollow $CaCO_3$ particles and the application as anticancer drug carrier. *Journal of the American Chemical Society*, 130, 47, (November 2008) pp. 15808-15810, ISSN 0002-7863

Whitesides, G. M. (2003). The 'right' size in nanobiotechnology. *Nature Biotechnology*, 21, 10, (September 2003) pp. 1161-1165, ISSN 1087-0156

Wong, J. E.; Gaharwar, A. K.; Müller-Schulte, D.; Bahadur, D. & Richtering, W. (2008). Magnetic Nanoparticle-Polyelectrolyte Interaction: A Layered Approach for Biomedical Applications. *Journal of Nanoscience and Nanotechnology*, 8, 8, (August 2008) pp. 4033-4040, ISSN 1533-4880

Xu, X. L. & Asher, S. A. (2004). Synthesis and utilization of monodisperse hollow polymeric particles in photonic crystals. *Journal of the American Chemical Society*, 126, 25, (June 2004) pp. l7940-7945, ISSN 0002-7863

Yang, H.; Liu, C.; Hui, Yang, D.; Zhang, H. & Xi, Z. (2009). Comparative study of cytotoxicity, oxidative stress and genotoxicity induced by four typical nanomaterials: the role of particle size, shape and composition. *Journal of Applied Toxicology*, 29, 1, (August 2009) pp. 69-78, ISSN 1099-1263

Yang, J.; Li, C. X.; Cheng, Z. Y.; Zhang, X. M.; Quan, Z. W.; Zhang, C. M. & Lin, J. (2007). *Size-tailored synthesis and luminescent properties of one-dimensional* Gd_2O_3*: Eu nanorods and microrods. Journal of Physical Chemistry C*, 111, 49, (November 2007) pp. 18148-18154, ISSN 1932-7447

Yuan, J. H.; Chen, Y.; Zha, H. X.; Song, L. J.; Li, C. Y.; Li, J. Q. & Xia, X. H. (2010). Determination, characterization and cytotoxicity on HELF cells of ZnO nanoparticles. Colloids and Surfaces B: Biointerfaces, 76, 1, (March 2010) pp. 145-150, ISSN 0927-7765

Zaveri, T.; Dolgova, N.; Chu, B. H.; Lee, J.; Lele, T.; Ren, F. & Keselowsky, B. G. (2009). *Proceedings of IFMBE*, pp. 119-120, ISSN 1680-0737, Miami, Florida, USA, May 2009, Springer, Berlin, Heidelberg

Zhang, K.; Holloway, T.; Pradhan, J.; Bahoura, M.; Bah, R.; Rakhimov, R. R.; Pradhan, A. K.; Prabakaran, R. & Ramesh, G. T. (2010). Synthesis and Magnetic Characterizations of $La_{1-x}Sr_xMnO_3$ Nanoparticles for Biomedical Applications. *Journal of Nanoscience and Nanotechnology*, 10, 9, (September 2010) pp. 5520-5526, ISSN 1550-7033

Zhang, K.; Holloway, T.; Bahoura, M.; Pradhan, A. K.; Prabakaran, R.; Pradhan, J.; Smith, S.; Hall, J. C.; Ramesh, G. T.; Sahu, D. R.; Huang, J.-L. (2009) Europium doped Gd_2O_3 and FeCo nanoparticles for biomedical application. *Proceedings of SPIE*, 7291, (March 2009) 729104-10, ISSN 0277-786X

Biomedical Engineering, Trends in Materials Science

Edited by Mr Anthony Laskovski

ISBN 978-953-307-513-6
Hard cover, 564 pages
Publisher InTech
Published online 08, January, 2011
Published in print edition January, 2011

Rapid technological developments in the last century have brought the field of biomedical engineering into a totally new realm. Breakthroughs in materials science, imaging, electronics and, more recently, the information age have improved our understanding of the human body. As a result, the field of biomedical engineering is thriving, with innovations that aim to improve the quality and reduce the cost of medical care. This book is the second in a series of three that will present recent trends in biomedical engineering, with a particular focus on materials science in biomedical engineering, including developments in alloys, nanomaterials and polymer technologies.

InTech Europe
University Campus STeP Ri
Slavka Krautzeka 83/A
51000 Rijeka, Croatia
Phone: +385 (51) 770 447
Fax: +385 (51) 686 166
www.intechopen.com

InTech China
Unit 405, Office Block, Hotel Equatorial Shanghai
No.65, Yan An Road (West), Shanghai, 200040, China
中国上海市延安西路65号上海国际贵都大饭店办公楼405单元
Phone: +86-21-62489820
Fax: +86-21-62489821